J. Renewable Sustainable Energy 16, 063307 (2024)
https://doi.org/10.1063/5.0238253

The eddies are attached, but it is all right.

Javier Jiménez[a)]
School of Aeronautics, Universidad Politécnica de Madrid, 28040 Madrid, Spain

(Dated: 12 December 2024)

The behavior of velocity fluctuations near a wall has long fascinated the turbulence community, because the prevalent theoretical framework of an attached-eddy hierarchy appears to predict infinite intensities as the Reynolds number tends to infinity. Although an unbounded infinite limit is not a problem in itself, it raises the possibility of unfamiliar phenomena when the Reynolds number is large, and has motivated attempts to avoid it. We review the subject and point to possible pitfalls stemming from uncritical extrapolation from low Reynolds numbers, or from an over-simplification of the multiscale nature of turbulence. It is shown that large attached eddies dominate the high-Reynolds-number regime of the near-wall layer, and that they behave differently from smaller-scale ones. In that limit, the near-wall layer is controlled by the outer flow, the large-scale fluctuations reduce to a local modulation of the near-wall flow by a variable friction velocity, and the kinetic-energy peak is substituted by a deeper structure with a secondary outer maximum. The friction velocity is then not necessarily the best velocity scale. While the near-wall energy peak probably becomes unbounded in wall units, it almost surely tends to zero when expressed in terms of the outer driving velocity.

I. INTRODUCTION

While there is reasonable agreement that turbulence should become independent of viscosity in the limit of very large Reynolds numbers[1,2], this is not true for wall-bounded turbulent flows, where even bulk quantities such as the friction factor slowly decay when the Reynolds number increases[3]. The reason is that there is a layer near the wall where viscosity is always needed to enforce the no-slip boundary boundary condition and, even if the relative thickness of this layer steadily decreases with the Reynolds number, the classical argument that leads to the logarithmic velocity profile[4] also implies that the velocity gradients grow without limit near the wall, and that their contribution to the production and dissipation of the turbulence fluctuations cannot automatically be neglected.

As a consequence of this singular behavior, much of the discussion about the high-Reynolds number limit of wall-bounded turbulence has centered on the intensity of the near-wall peak of the streamwise velocity fluctuations, u'_p, empirically located at a distance $y_p^+ \approx 15$ from the wall, where the '+' superindex denotes 'wall' normalization with the friction velocity u_τ and with the kinematic viscosity ν. In numerical simulations, its magnitude approximately increases logarithmically with the friction Reynolds number, $Re_\tau = u_\tau h/\nu$, where h is the flow thickness[5]. The evidence from experiments is more mixed, but not incompatible with numerics when both are available[5–7], and a similar logarithmic behavior is found in the spanwise velocity and in the pressure, although not in the fluctuations of the wall-normal velocity[5]. The implication that the velocity fluctuations become infinitely strong in the limit of infinitely high Reynolds number has caused some unease, leading to repeated efforts to avoid it[8–10] and to restore the asymptotic Re_τ-independence of wall turbulence.

This paper briefly reviews those efforts. One of our first conclusions will be that the available range of experimental and numerical Reynolds numbers is too narrow for an unguided extrapolation to $Re \to \infty$, and is likely to remain so for some time. The decision between different models should rather come from theoretical arguments, if possible, and most of the paper deals with how such theoretical models are constrained by the data. We denote the streamwise, wall-normal and spanwise directions by x, y and z, respectively, and the corresponding velocity components by u, v and w. Capital letters denote y-dependent ensemble averages, $\langle\,\rangle$, as in the mean velocity profile, $U(y)$, and lower-case ones are fluctuations with respect to these averages. Primes refer to root-mean-square (rms) fluctuation intensities.

In principle, an infinitely strong near-wall intensity peak does not present insurmountable theoretical difficulties. If we assume an approximately constant tangential Reynolds stress throughout the logarithmic layer, $\langle uv\rangle \approx -u_\tau^2$, and a logarithmic profile for the mean velocity[3],

$$U^+ = A + \kappa^{-1}\log y^+, \tag{1}$$

where $A \approx 5$, and $\kappa \approx 0.4$ is the Kármán constant, the total energy production in the flow is[3]

$$-\int_0^h \langle uv\rangle\,\partial_y U\,\mathrm{d}y \approx \int_{\delta_{in}}^{Re_\tau} \frac{u_\tau^3\,\mathrm{d}y^+}{\kappa y^+} \sim \frac{u_\tau^3}{\kappa}\log Re_\tau, \tag{2}$$

which grows without bound with Re_τ. The reason for the singularity is not the lower bound of the integral in (2), which can be regularized by a suitable viscous cutoff, but the divergence of the integral of the mean shear, $\partial_y U \sim O(1/y)$, in its upper limit, $O(h^+ = Re_\tau)$. Unless the logarithmic profile is assumed to cover a vanishingly small fraction of the flow thickness as Re_τ increases, Eq. (2) implies an infinitely large production of energy, at

a)jjsendin@gmail.com

least when expressed in wall units, that could conceivably leak towards the wall and result in infinitely strong fluctuations in its neighborhood. Note, in particular, that the bulk velocity from Eq. (1), which arguably drives the flow, also becomes infinite as $Re_\tau \to \infty$.

However, it is probably true that such a situation would result in extremely strong fluctuations near the wall when Re_τ is large but finite. There is some evidence of strong fluctuations in the atmospheric boundary layer[11,12] but, even in that case, their intensity, $u_p'^+ \approx 4$ at $Re_\tau \sim O(10^6)$, is weak with respect to the mean velocity at the same distance from the wall $U^+(y_p) \approx 10.5$. In fact, even using the most unfavorable of the extrapolations discussed below for $u_p'^+$, the intensity of the near-wall fluctuation peak only becomes comparable to the mean profile for $Re_\tau \approx 10^{74}$, which is well beyond any reasonable extrapolation from experimental or observational Reynolds numbers. More damaging from the theoretical point of view is the assumption that the viscosity required to enforce the boundary conditions remains relevant for infinitely strong velocity structures, and that the associated flow features remain stable.

A recent survey and discussion of currently popular models can be found in Ref. 10, and will not be repeated here. They can broadly be classified in two groups. The first one are structural models that propose mechanisms for how the flow is organized. The best-known is the attached-eddy model, first proposed by Townsend [13], and structurally developed by many others[14–17]. It is the main support for the unbounded logarithmic growth of the near-wall intensity, and will be discussed later in more detail. The models in the second group typically assume a finite intensity asymptote at $Re_\tau \to \infty$, and search for the most mathematically and physically consistent form of the defect with respect to this asymptote. The two best-known proposals are a logarithm[9,10,18],

$$u_p'^2(Re_\tau) = u_p'^2(\infty) - O(1/\log Re_\tau), \tag{3}$$

and a power law[8,19],

$$u_p'^2(Re_\tau) = u_p'^2(\infty) - O(Re_\tau^{-1/4}), \tag{4}$$

which are, unfortunately, difficult to distinguish within the available range of Reynolds number. In this paper, we will mostly restrict ourselves to exploring the consequences of the attached-eddy model, both from the point of view of the near-wall fluctuations and of its interplay with the viscous boundary condition.

We will do this by comparing theoretical arguments with a homogeneous set of data presented in §II. The attached-eddy model and its supporting evidence are discussed in §III, and its weak points are discussed in §IV, together with possible solutions. This first part of the paper deals mostly with the fluctuations of the streamwise velocity component, but §V extends the argument to the spanwise velocity. Conclusions are summarized in §VI.

TABLE I. Numerical data sets most often used in the paper. The box dimensions are $L_x \times 2h \times L_z$, and the symbols in the rightmost column are used consistently in the figures.

Reference	L_x/h	L_z/h	Re_τ	Symbol
del Álamo *et al.* [20]	8π	3π	180–950	○
Hoyas and Jiménez [21]	8π	3π	2000	○
Lozano-Durán and Jiménez [22]	60π	6π	550	□
Lozano-Durán and Jiménez [22]	2π	π	4200	□
Bernardini *et al.* [23]	6π	2π	180–4000	△
Lee and Moser [24]	8π	3π	550–5200	◇
Hoyas *et al.* [25]	2π	π	10000	▽

TABLE II. Coefficients for the line fits in Fig. 1.

	A_L, B_L	A_{dP}, B_{dP}	A_{dL}, B_{dL}	A_S, B_S
u'^2	3.75, 0.63	11.5, -19.3	13.8, -40.0	4.17, 0.57
w'^2	-0.97, 0.44	3.9, -10.0	5.18, -20.9	-0.18, 0.34

II. THE DATA SET

We will mostly restrict ourselves to numerical doubly periodic pressure-driven turbulent channel flow between parallel plates separated by $2h$, for which there is a reasonably homogeneous set of simulations spanning two orders of magnitude in Reynolds number. They are summarized in Tab. I. At the same time, these simulations include enough variety of computational parameters, mainly in the numerical method and in the size of the computational box, to provide some safeguard against overfitting our results to one particular technique. Although restricting us in this way limits our conclusions somewhat, it avoids the scatter due to variable resolution in experiments, while keeping a range of Re_τ comparable to what can reliably be measured experimentally. Moreover, since our discussion will lead us to consider the effect on the near-wall region of the largest flow scales, the restriction to channels avoids the known differences between their large scales and those in pipes[26] or in boundary layers[18,27,28]. Most data sets in table I include mean fluctuation profiles, one- and two-dimensional spectra, and energy balances, and are freely accessible from the web pages of the different groups.

Spectra and cospectra are used in premultiplied form, $\Phi_{ab}(k_x, y) = k_x \langle \hat{a}\hat{b} \rangle$, where $\hat{a}(k_x)$ is the Fourier coefficient of the expansion of $a(x)$ in terms of the streamwise wavenumber k_x, with similar definitions for spanwise spectra in terms of k_z, and for two-dimensional ones in terms of both wavenumbers. They will usually be expressed as functions of the wavelengths, $\lambda_j = 2\pi/k_j$.

The fluctuation profiles and peak intensity of the two wall-parallel velocities are given in Fig. 1, which shows that they agree reasonably well among different data sets at similar Reynolds numbers. The growing trend of the

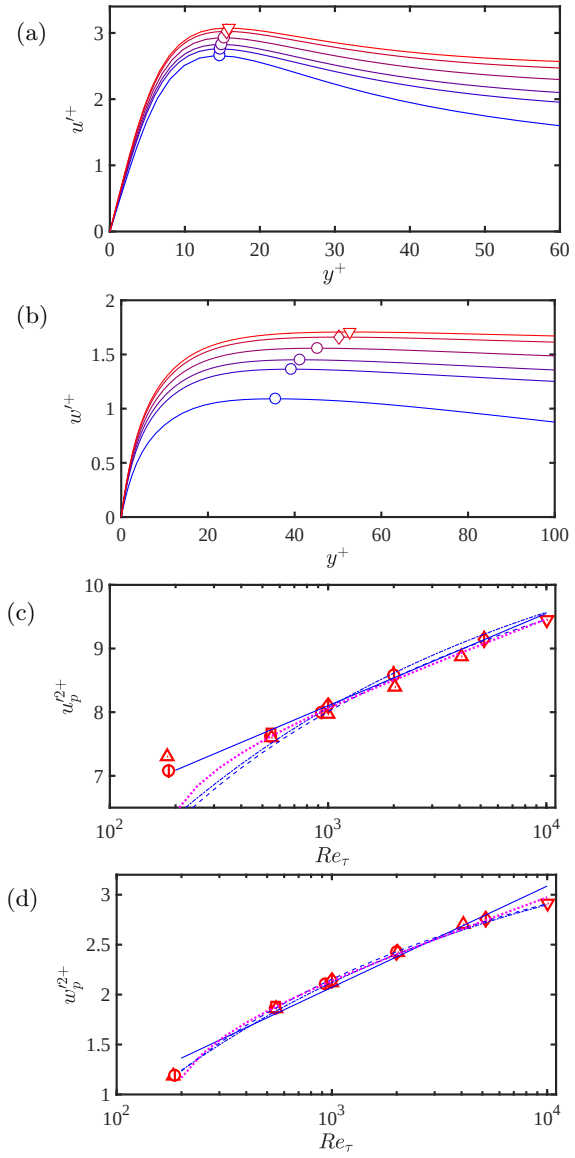

FIG. 1. (a) Intensity of the streamwise velocity fluctuations near the wall. The symbols mark the position of the near-wall peak, as in table I. Numerical channels[24,25,29]. The Reynolds number increases from blue to red in $Re_\tau = 180 - 10^4$. (b) As in (a), for the spanwise velocity. (c) Peak intensity of the streamwise velocity fluctuations near the wall as a function of the Reynolds number. Symbols as in table I, with standard deviations as vertical bars when available. (d) As in (c), for the spanwise velocity. Lines are different data fits: ———, Logarithmic approximation[13], $u_p'^{2+} = A_L + B_L \log(Re_\tau)$; – – –, power defect law[8], $u_p'^{2+} = A_{dP} + B_{dP} Re_\tau^{-1/4}$; -·-·-, logarithmic defect law[10], $u_p'^{2+} = A_{dL} + B_{dL}/\log(Re_\tau)$; ·····, shifted logarithm, $u_p'^{2+} = A_S + B_S \log(Re_\tau - 150)$. Coefficients are collected in table II.

profiles is clear in Figs. 1(a,b), as is the trend of the peak position to slowly move away from the wall when the Reynolds number increases (for which there is also some experimental evidence[30]).

The peak intensities are collected in Figs. 1(c,d), with line fits from the models discussed above, with coefficients either taken from the original publications or fitted numerically to the data. They separate in two groups. The straight line is the basic logarithm already discussed above for the attached-eddy model[5,21], which predicts an infinite intensity as $Re_\tau \to \infty$. The second group includes the dashed and chaindotted curves in each figure[8,10], both of which assume a finite limit for the intensity, as in Eqs. (3) and (4). The defect formulations appear to represent the data better than the straight line of the logarithm, especially if we disregard the lowest Reynolds number, $Re_\tau \approx 180$, but the most striking observation is how similar to each other they are. Finally, the red dotted lines in the two figures are a shifted logarithm with a virtual origin for Re_τ, which predicts an unbounded peak at large Re_τ. It is not intended as a serious proposal, and I am not aware of any theoretical basis for it (although neither is it absurd to shift the Reynolds number by a transition threshold), but it shows that there are simple approximations that fit the available data as well as the defect laws, while predicting an infinite limiting value for the near-wall peak. It emphasizes that simple curve fitting cannot decide the issue.

It may be relevant at this point to estimate which would be the Reynolds number required to distinguish between the different fits in Figs. 1(c,d). An order of magnitude could be how far the logarithmic straight line has to be extended before it reaches the asymptotic value of any of the two defect laws. The details depend on the approximation and on the variable chosen, but it is in all cases of the order of $Re_\tau \approx 10^5$. This is at least 15–20 years in the future for numerical simulations, but it is worth remarking that experiments in pipes[30] up to $Re_\tau \approx 4 \times 10^4$ have proved inconclusive for this purpose[10], and that data from the atmospheric surface layer at $Re_\tau = O(10^6)$, although not strictly a channel, appear to follow the logarithmic trend reasonably well[11].

III. THE ATTACHED-EDDY MODEL

The key theoretical contribution to understanding the velocity fluctuations was made by Townsend[13], who noted that the usual argument that there is an overlap layer in which neither the viscous unit of length nor the flow thickness are relevant[4] should also apply to them. Although the resulting attached-eddy model has been reviewed often, we will recall it here to identify where the logarithmic prediction could go wrong.

The naive argument is that, if there is no scale for lengths, but u_τ is a scale for the velocities, the functional dependence of any variable with dimensions of velocity on a variable with dimensions of length should be logarithmic (see appendix A in Ref. 5). We could thus expect that $u'/u_\tau \sim \log(y/h)$, which, when particularized at a fixed inner viscous limit, y_p^+, results in $u_p'/u_\tau \sim \log Re_\tau$.

There is substantial experimental and numerical ev-

idence for both approximate logarithmic behaviors[31], which, as mentioned above, extend to the fluctuations of the pressure and of the spanwise velocity[32] but, in the absence of a rigorous theory, it is always possible that higher Reynolds numbers than those currently available may lead to something different.

Moreover, there are logical flaws in the previous argument. Most obviously, an argument similar to the one used for u' applies to any power of the velocity, and some selection rule is needed to decide which power to use. In addition, some reason needs to be found for why the logarithmic behavior applies to u' and w' but, as mentioned above, not to v', and a justification is required for why u_τ is the right scaling unit for the velocity fluctuations.

In general, it is unwise to use similarity arguments without a dynamical model, and Townsend [13] proposed that the logarithm is implemented by the superposition of a self-similar family of 'attached' Reynolds-stress-carrying eddies linking the wall to the interior of the flow. In the absence of a fixed length scale, their height is proportional to their wall-parallel size (λ_x or λ_z), while their intensity is $O(u_\tau)$ because each eddy family is responsible for carrying the tangential Reynolds stress ($-uv$) at one distance from the wall. This is supported by observations: the solid contours in Figs. 2(a,b) are the premultiplied cospectra, $\Phi^+_{uv}(k_x)$ and $\Phi^+_{uv}(k_z)$ of the tangential Reynolds stress, respectively drawn as functions of y and of the streamwise or spanwise wavelengths. The contours are normalized with the friction velocity, and the figures show that a stress $-uv \sim O(u_\tau^2)$ is concentrated along a spectral ridge in which $\lambda_x \approx 25y$ and $\lambda_z \approx 5y$, and which extends from a minimum wavelength that scales in wall units to an outer one that scales with h. Since it can be shown that the streamwise and wall-normal velocities are well correlated in the regions of the $\lambda - y$ plane where the Reynolds stresses are substantial, this extends the role of u_τ from a velocity scale for the overall intensity to one for individual spectral bands, although the argument may not apply to 'sterile' scales without tangential stress.

Because there is no fixed length scale, these bands are logarithmic (e.g. from λ_x to $2\lambda_x$), and the number of eddy families found at a given distance y from the wall is the number of logarithmic bands required to cover the range of lengths from y to the flow thickness, $O(h)$, which increases logarithmically with h/y. If we further assume that the velocity fluctuations of the different bands are uncorrelated, their variances add, resulting in a logarithmic behavior with the Reynolds number for $u'^{2+}(y) \sim \log(y/h)$ and for $u'^{2+}(y_p)$. Townsend [13] distinguishes between 'inactive' attached variables, such as u' and w', which are not sufficient to generate tangential Reynolds stress and are only damped by the wall in a thin viscous layer, and 'active' ones, like v', that contribute to the stress but are inhibited by impermeability at distances from the wall comparable to their size. Only the former should have logarithmic profiles.

The difference between the two types of variables can

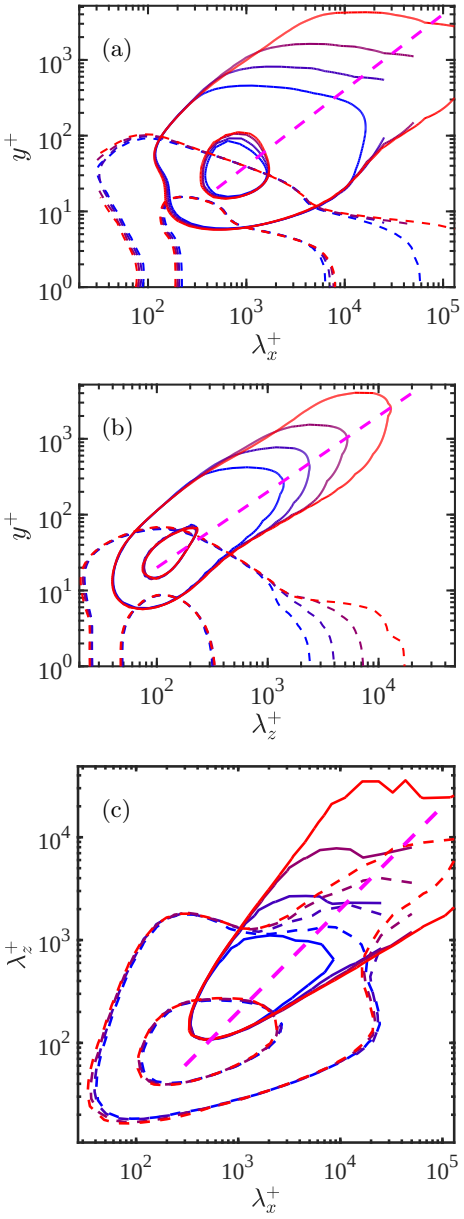

FIG. 2. (a) Solid contours are premultiplied cospectra of the tangential Reynolds stress, $-\Phi^+_{uv}(\lambda_x, y) = [0.2, 0.8]$ times the common maximum of the four cospectra. Dashed ones are premultiplied spectra of the spanwise vorticity, $\Phi^+_{\omega_z\omega_z}(\lambda_x, y) = [0.05, 0.4]$ the common maximum. The dashed diagonal is $\lambda_x = 25y$. (b) As in (a), but as functions of λ_z. The dashed diagonal is $\lambda_z = 5y$. (c) Two-dimensional integrated spectra as functions of (λ_x, λ_z): Solid contours are $-\int \Phi^+_{uv}\, \mathrm{d}y^+$ integrated over $y \in [0.005, 0.5]\lambda_x$. Contours are [0.2, 0.8] the common maximum. Dashed contours are premultiplied spectra of the spanwise vorticity, $\int \Phi^+_{\omega_z\omega_z}\, \mathrm{d}y^+$, integrated over $y^+ \in [0, 20]$. Contours are [0.05, 0.4] the common maximum. The dashed diagonal is $\lambda_x = 5\lambda_z$. Numerical channels[22,24], with the Reynolds number increasing from blue to red: $Re_\tau = 550, 1000, 2000, 5200$.

be seen in Figs. 2(a,b), where the dashed isolines are spectra of the spanwise vorticity. Bradshaw [33] argued that, in the absence of other terms of the momentum equation, the flow at long wavelengths, and at distances from the wall below the Reynolds-stress ridge, can only be driven by the pressure footprint of active eddies further from the wall and should therefore be essentially irrotational. It is indeed clear from 2(a,b) that wavelengths longer than $\lambda_x^+ \approx 10^4$ are approximately irrotational above $y^+ \approx 10$, and Fig. 12(d) in Ref. 5 shows that the pressure is a deep variable, correlated from the wall to the Reynolds-stress ridge. But potential flow cannot satisfy the no-slip condition at the wall, and a viscous rotational layer appears at long wavelengths below $y^+ \lesssim 10$. Since $\omega_z \approx -\partial_y u$ in that region, this implies that non-trivial fluctuations of u reach the vicinity of the wall at those wavelengths.

The solid contours in Fig. 2(c) are two-dimensional Reynolds-stress cospectra integrated over the active band of wall distances corresponding to each wavelength, and the dashed ones are spectra of the spanwise vorticity integrated over the viscous near-wall layer. The figure strongly supports that the latter are the effect of the detached Reynolds stresses, although not necessarily at the same distance from the wall for all wavelengths. The same is implied by the advection velocity of the long wavelengths near the wall, which is not the local mean flow velocity[5,34], but the velocity at $y/h \approx 0.3 - 0.4$. However, the conclusion that they are driven by pressure is less clear. Pressure correlations only attach to the wall for $\lambda_x/h \lesssim 4$, and cannot therefore drive longer wavelengths[28]. In fact, it will be seen below that those scales are better described as internal turbulent layers, presumably driven from above by turbulent diffusion[5].

Families of self-similar attached eddies, as well as the distinction between active and inactive motions, have been observed and characterised in some detail numerically[5,20,35] and experimentally[17,36–38].

There are several debatable points in these arguments, most of which have been discussed in the literature and will not be repeated here, but some of which deserve closer attention. A well-known limitation of the attached-eddy model is that it does not include viscosity, whose effects are lumped in the rule that something happens below $y_p^+ = 15$. This has occasionally been suggested as responsible for scaling failures[10]. We have seen that what viscosity does is to generate the thin vortex layers in Fig. 2, but how they are maintained, their dimensions, and their effect are unclear, and we mentioned in the introduction that their stability is problematic if the fluctuations become too strong.

However, the overall conclusion from the previous discussion remains that the reason why velocity fluctuations do not scale well is that they contain a wide range of wavelengths, even when they are very close to the wall. This often-made point[14,15,21,39] is clear from the spectra in Fig. 3 of the near-wall streamwise velocity at $y_p^+ = 15$. There is a universal 'core', centered at

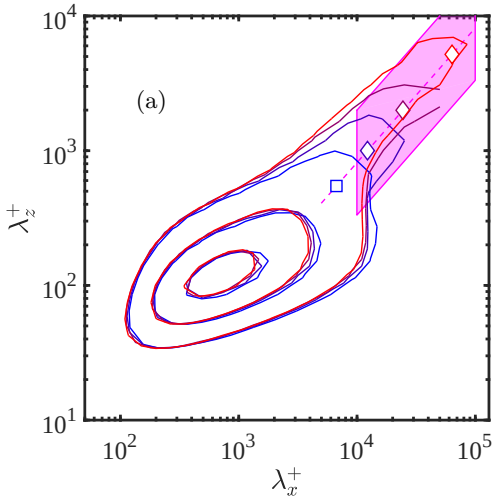

FIG. 3. Premultiplied energy spectrum of the streamwise velocity, Φ_{uu}^+ at $y^+ = 15$, versus the wall-parallel wavelengths. Numerical channels[22,24], with the Reynolds number increasing from blue to red: $Re_\tau = 550$, 1000, 2000, 5200. Contours are [0.15, 0.4, 0.8] times the common maximum of the four spectra. The dashed diagonal is $\lambda_x = 12\lambda_z$, and symbols are $\lambda_z = h$. The translucent patch is used in Fig. 5.

$\lambda_x^+ \times \lambda_z^+ \approx 1000 \times 100$, which does not reach above $y^+ \approx 100$ (Fig. 2) and collapses well across Re_τ. That its dimensions scale in wall units shows that it is controlled by viscosity[40–42], but it is accompanied by larger-scale spectral tails that extend to $\lambda \sim O(h)$, and which are responsible for the extra energy of the overall fluctuations. The dynamics of these tails, which does not have to be the same as for the viscous core, has to be studied if the overall peak intensity is to be understood.

This wide range of scales is a problem for asymptotic models that seek to represent the flow in terms of an outer 'regular' turbulence and a small-scale object near the wall, since the latter does not exist as such in real flows. In fact, given that the total peak energy includes contributions from a wide range of wavelengths, it is unclear whether it makes sense to speak of a single velocity and length scale for it.

IV. THE LARGE SCALES

Figures 4(a,c) are similar to the cospectra in Figs. 2(a,b), but drawn for the streamwise velocity component. To facilitate comparison, the dashed diagonals in the two figures are the same, and show that the upper limit of the kinetic energy and of the Reynolds stress are similar, but it is clear from Figs. 2 and 4 that the streamwise velocity spectrum extends to the wall, while the cospectrum stays away from it. Notice, in particular, the different behavior of the larger wavelengths.

Figure 4 includes as thick dashed lines and symbols the wall-normal location of the maximum of Φ_{uu} at each

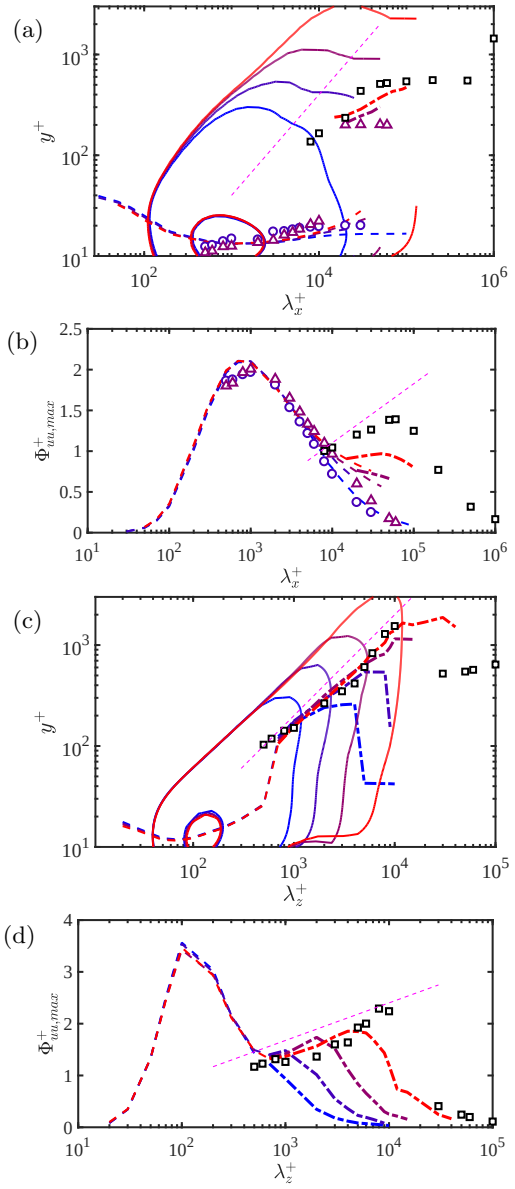

FIG. 4. (a,c) Contours are the premultiplied spectrum of the streamwise velocity. The contours are [0.2, 0.8] times the overall maximum of all the Φ^+_{uu}. Dashed and chain-dotted lines are the location of the inner and outer maxima of Φ_{uu} at each wavelength. Numerical channels[22,24], with the Reynolds number increasing from blue to red: Re_τ = 550, 1000, 2000, 5200. Symbols are boundary layers from Ref. 43: ○, Re_τ = 1014; △, 1844; or from Ref. 17, □, Re_τ = 14000. (b,d) Maximum of Φ^+_{uu} versus wavelength, with the same lines and symbols as above. (a,b) Against λ_x. (c,d) Against λ_z. The dashed magenta line in (a) and (c) are $\lambda_x^+ = 25y^+$ and $\lambda_z^+ = 5y^+$, respectively. The ones in (b) and (d) are $\Phi^+_{uu,max} = 0.315\log(\lambda_x^+) - 1.8$ and $\Phi^+_{uu,max} = 0.315\log(\lambda_z^+) - 0.5$.

wavelength. We saw when discussing Fig. 1 that the energy peak drifts slowly away from the wall with the Reynolds number, and Figs. 4(a,c) show a clearer dependence on the wavelengths. The symbols are from experimental boundary layers[17,43] and, although sparser near the wall, are compatible with the numerics. The inner maximum at the shorter wavelengths marks the edge of the viscous layer, and is superseded beyond $\lambda_x^+ \approx 10^4$ by an outer maximum located at $y_{max} \approx \lambda_z/5$ or $\lambda_x/25$ (Fig. 4a,c). Note that this implies that the transition to an outer peak always takes place when $y^+_{max} \approx 200$, which can be interpreted as the thickness at which the near-wall viscous layers become unstable.

The amplitude of these maxima is shown in Figs. 4(b,d). It collapses well with Re_τ in the viscosity-dominated region, $\lambda_x^+ \lesssim 10^4$ or $\lambda_z^+ \lesssim 10^3$, but not at the larger wavelengths associated with the outer maximum. Their growth with λ can be interpreted as a wavelength-by-wavelength counterpart to the logarithmic growth of $u_p'^2$ with Re_τ, represented here by the range of wavelengths over which the one-dimensional spectrum is summed. We have added to Figs. 4(b,d) logarithmic approximations to this growth, using half the slope in Fig. 1 for $u_p'^2$, on the assumption that half of the peak growth is due to the wider range of λ_x and the other half to the wider range of λ_z. These logarithms match the data relatively well, but they should only be considered as aids to the eye, subject to the same caveats as the curve fits in Fig. 1(a,b).

Fortunately, more can be said about the large flow scales. The outer maximum of the longest structures in Fig. 4(a) represents layers of dimensions $(\lambda_x \times y \times \lambda_z)^+ = O(20000 \times 500 \times 4000)$, which are thin both with respect to the channel height ($Re_\tau = 5200$) and to their own length. They are also deep enough to be fully turbulent. Internal turbulent layers are common when wall-bounded flows cross boundaries between different types of wall or are otherwise perturbed, and have been extensively studied in meteorology[44,45] and for heterogeneous surfaces[46]. Using a rough approximation[45], there is an internal equilibrium layer (EL) whose thickness after time Δt grows to $\delta_{EL} \approx u_\tau \Delta t/4$, and satisfies the universal velocity profile corresponding to the friction velocity that develops after the perturbation. Since the lifetime of the stress-carrying structures is[47] $\Delta t \approx \Delta y/u_\tau \approx \lambda_z/u_\tau$, the thickness of the EL generated by perturbations of width λ_z is $\delta_{EL} \approx \lambda_z/4$, which approximately agrees with the location of the outer maximum in Fig. 4(c) .

The model is that large-scale fluctuations with wavelengths of the order of $\lambda_x^+ \approx 5\lambda_z^+ \gtrsim 10^4$ (Fig. 2c) are equilibrium turbulent boundary layers satisfying the universal profile $U = u_\tau F(y^+)$ with a perturbed friction velocity, and that, if they are viewed as perturbations to the overall mean velocity, they can be modeled as weak perturbations of $u_\tau \to u_\tau + \delta u_\tau$. Upon linearization,

$$(\delta U) = (\delta u_\tau)(F + y^+ \mathrm{d}F/\mathrm{d}y^+) \equiv (\delta u_\tau) G(y^+), \qquad (5)$$

which links the rms intensity of the velocity fluctuations

to the rms perturbation of the friction velocity, $(\delta u_\tau)' = u_*$. In the viscous layer, $F = y^+$, and

$$(\delta U)'/u_* = 2y^+. \tag{6}$$

This is essentially the modulation described in[48], which was shown in[49] to reduce in the buffer layer to a modulation of u_τ. We extend it here to the logarithmic layer, where F satisfies (1), and

$$(\delta U)'/u_* = \kappa^{-1}\left(1 + A\kappa + \log y^+\right). \tag{7}$$

These equations are tested in figure 5(a) for spectral densities within the patch of large-scale tails in Fig. 3. The perturbation intensity, u_*, of the friction velocity has been adjusted for each wavelength to fit Eq. (5) to the spectral profile from the wall to the location of the spectral maximum, but the definition of F has not been modified. The symbols in Fig. 5(a) are $G(y^+)$ in Eq. (5), computed from the mean velocity $F(y^+)$ of a turbulent channel, and the agreement is excellent, supporting the assumption of turbulent equilibrium internal layers. Note that the lowest $Re_\tau = 550$ is not in the figure because it never develops an outer peak. This model was probably first used by Bradshaw [33] to explain the differences between boundary layers subject to different streamwise pressure gradients. Some time later, Spalart [50] tested it on simulations of a zero-pressure-gradient boundary layer at $Re_\tau \approx 400$, and concluded that its large scales were better represented by laminar oscillating Stokes layers, but the comparison with Fig. 4 shows that his Reynolds number was too low, and his wavelength too short ($\lambda_x^+ \approx 10^3$), falling in the viscous range of Fig. 4(a).

More recently, Pirozzoli [19] has applied the equilibrium layer model to pipes, with results similar to Fig. 5. However, the amplitude of his perturbations depends on λ^+, while Fig. 5(b) shows that u_* scales with λ_x/h rather than in wall units. The reason for this discrepancy is unknown, and deserves further investigation. The rms of the fluctuations of u_τ tend to some non-zero value when $\lambda_x \to 0$, so that the fluctuation velocity profile can be approximated as

$$u'^{2+}(y^+) = u_s'^{2+}(y^+) + G^{2+}(y^+)\int_{\lambda_1/h}^{\lambda_2/h} u_*^{2+}(\lambda/h)\,\mathrm{d}\log\lambda, \tag{8}$$

where $G(y^+)$ is defined in Eq. (5), $\lambda_1 = \max(\lambda_{in}, 25y)$, and $u_s'^{2+}$ is the contribution of scales whose λ_x is shorter than the wavelength, λ_{in}, at which the viscous sublayer becomes unstable and fluctuations have to be modeled as turbulent profiles. It is important to note that the lower limit of this integral scales in wall units ($\lambda_{in}^+ \approx 2\times 10^4$ in Fig. 4), while the upper one either extends to infinity, or scales in outer units ($\lambda_2 = 25h$ in our case, because of the length of our computational box). Assuming that the small-scale contribution to Eq. (8) is independent of Re_τ, and that the integral of u_*^2 stays bounded at $\lambda \to \infty$, the dominant contribution to Eq. (8) at high Re_τ comes from the lower limit of the integral,

$$u'^{2+}(y^+) \approx u_s'^{2+}(y^+) + G^{2+}(y^+)u_*^{2+}(0)\log(Re_\tau/\lambda_{in}^+). \tag{9}$$

It is important to realize that $U + \delta U$ in Eq. (5) is the mean profile of a perturbed boundary layer. These faster- or slower-than-average local equilibrium layers have their own small-scale perturbations that are modulated by the outer Reynolds-stress structures, but those are second-order effects, negligible with respect to the mean profile. The maximum fluctuation intensity at the inner energy peak is $u_p'^{2+} \approx 9$ in our data base, while the mean velocity at that point is $U^{2+}(y_p) \approx 100$. The fluctuation profiles are only relevant if the mean profile can be considered fixed, but any perturbation of the latter overwhelms the modulation of the small scales.

Eq. (9) is also a logarithm that diverges as $Re_\tau \to \infty$, but its most interesting aspect is that the form of the large-scale correction is not a peak near the wall, but something similar to the mean velocity profile of a regular boundary layer, so that the fluctuation peak will be absorbed into something closer to a plateau at high Re_τ. Although estimating this behavior necessarily implies extrapolation from lower Reynolds numbers, Fig. 5(c) plots Eq. (8) for several large Re_τ. The lowest curve in the figure, $Re_\tau = 1000$ is used to estimate the viscous contribution, u_s', displayed in the figure as a dashed line, and is therefore automatically fitted. But the corrections for the rest of the curves are computed by estimating the integral in Eq. (8), using a lineal least-square approximation to u_* in Fig. 5(b). The agreement with our highest Reynolds number, $Re_\tau = 10^4$ is excellent, and it is intriguing that the uppermost curve in the figure, intended to approximate data from the atmospheric surface layer[12], also appears to fit well. The fluctuation profile in this case is already very different from that at lower Reynolds numbers, including a second outer maximum of u' that requires experimental confirmation. Although the implied $Re_\tau = O(10^6 - 10^7)$ are well in the future for laboratory or numerical flows, they are not out of range for geophysical ones[11,12]. In fact, some measurements in the atmospheric surface layer show a clear double peak in the profile of u', but there is some uncertainty as to whether this may be partly due to damping of the near-wall peak by roughness, buoyancy, or instrumental effects[51].

V. THE SPANWISE VELOCITY

Up to now we have mostly dealt with the streamwise velocity fluctuations, but it is clear from Fig. 1 that the spanwise velocity also has a potentially infinite limit. Figure 6 displays the two-dimensional spectrum of w', and shows that the reason is also the effect of large structures. Their maximum size also scales with h rather than in wall units, but they are wide rather than long, as required by continuity[52].

The perturbation expansion is also slightly different

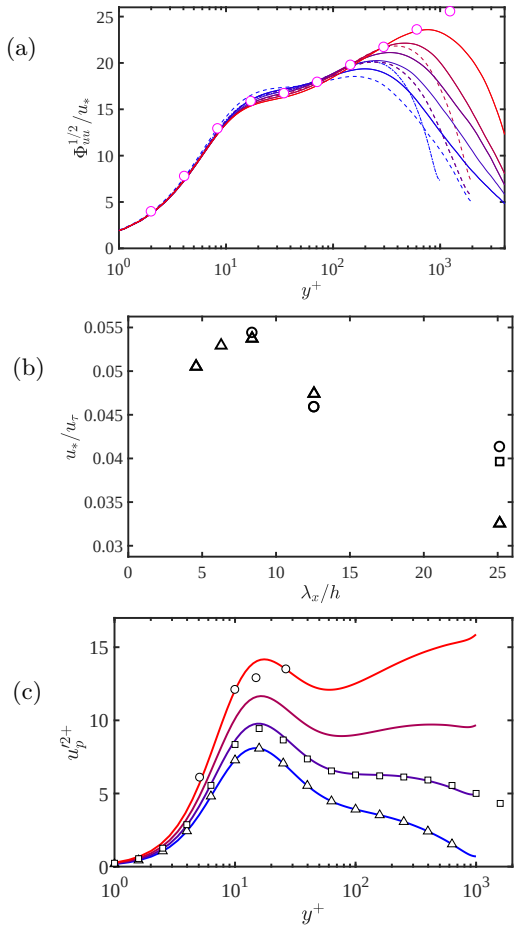

FIG. 5. (a) Spectral density of the streamwise velocity for various wavelengths, from $\lambda_x^+ = 2\times10^4$ to $\lambda_x = 25h$, from blue to red, integrated in λ_z over the diagonal band in Fig 3, defined as $\lambda_z \in \lambda_x/[30, 5]$. The symbols are G in Eq. (5), computed from the mean velocity profile in[24]. (b) Friction velocity perturbation intensities obtained from fitting (a). Channels[24]: (–·–·– and □) $Re_\tau = 1000$; (– – – and ○) $Re_\tau = 2000$; (——— and △) $Re_\tau = 5200$. (c) Lines are fluctuation profiles estimated from Eq. (8). From bottom to top: $Re_\tau = 1000$, 10^4, 10^5 and 2×10^6. Symbols are channel simulations[24,25] and the atmospheric surface layer[12] at those Reynolds numbers. The dashed line is $u_s'^{2+}$, estimated from $Re_\tau = 1000$.

from the streamwise component. The first term in the expression for G in Eq. (5) comes from the incremental boundary layer created by the perturbation of u_τ, which in this case has to be oriented spanwise. The second term is the deformation of the existing boundary layer by the change in length scale due to the new u_τ, and is missing from δW, for which no preexisting spanwise flow exists. The fluctuation equation becomes,

$$(\delta W)' = (\delta w_\tau)' F(y^+) = w_* F(y^+), \qquad (10)$$

where $F(y)$ is, as before, the mean velocity profile of a regular channel, and the symbols w_τ and w_* have been introduced to represent the friction velocity of the spanwise perturbation flow.

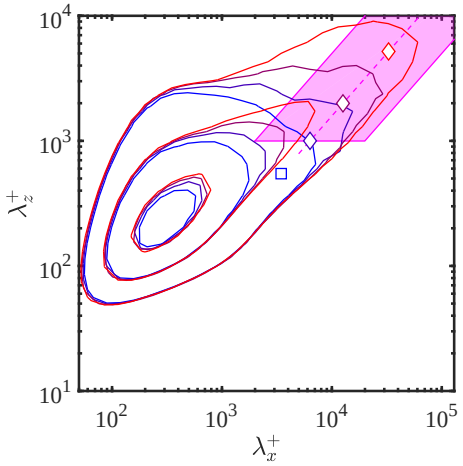

FIG. 6. Premultiplied energy spectrum of the spanwise velocity, Φ_{ww}^+ at $y^+ = 50$, versus the wall-parallel wavelengths. Numerical channels[22,24] with the Reynolds number increasing from blue to red: $Re_\tau = 550$, 1000, 2000, 5200. Contours are [0.15, 0.4, 0.8] of the common maximum of the four spectra. The dashed diagonal is $\lambda_x = 6\lambda_z$ and symbols are $\lambda_z = h$. The translucent patch is used in Fig. 7(c,d).

Figure 7 summarizes, for the spanwise velocity, the same information as Figs. 4 and 5 do for u. As in the previous case, the relevant result is that the transition from the inner to the outer peak scales in wall units, at approximately the same wavelength as for the streamwise velocity, $\lambda_z^+ \approx 1000$ (Fig. 7a,b). Figure 7(d) shows that the perturbation w_* required to fit the profiles in Fig. 7(c) to Eq. (10) scales well in outer units, so that the total energy also diverges logarithmically. Notice that the fit of Eq. (10) to the data in Fig. 7(c) is as good as that in Fig. 5, even if the two predicted profiles are fairly different.

There are some differences between the two velocity components. The Φ_{ww} spectra in Fig. 7(a) are consistently wider and taller than Φ_{uu} in Fig. 4(c). The outer peak of Φ_{ww} follows $\lambda_z \approx 10y$ instead of $\lambda_z \approx 5y$, and the distinction between inner and outer intensities in Fig. 7(b) is much less clear than in Fig. 4(d). While the inner and outer peaks of Φ_{uu} are often two distinct maxima separated in y, those of Φ_{ww} are a single maximum whose location depends on λ. There are essentially no bimodal intensity profiles in Φ_{ww}.

The distribution of perturbation friction velocities is also different in the two cases. Although both scale in outer units, the distribution in Fig. 5(b) is fairly smooth, with what appears to be a definite limit at $\lambda_x = 0$, but Fig. 7(d) could have a more singular limit at that point.

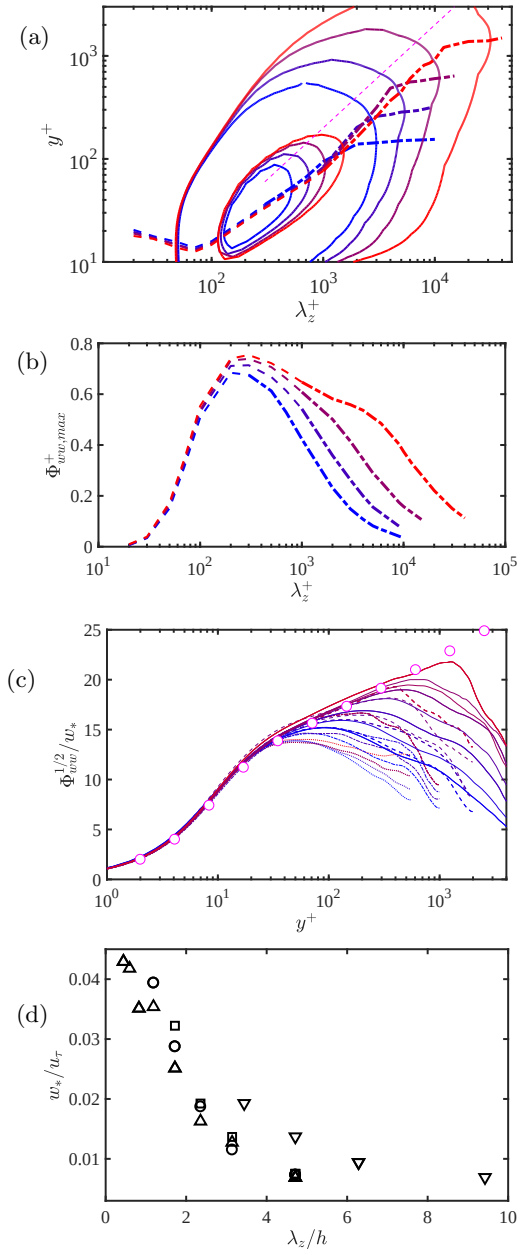

FIG. 7. (a) Premultiplied spectrum of the spanwise velocity versus λ_z. The contours are [0.2, 0.8] times the overall maximum of all the Φ^+_{ww}. Dashed and chaindotted lines are the location of the inner and outer maxima of Φ_{ww} at each wavelength. Numerical channels[22,24], with the Reynolds number increasing from blue to red: $Re_\tau = 550, 1000, 2000, 5200$. The dashed magenta line is $\lambda_z^+ = 5y^+$. (b) Maximum of Φ_{ww} versus wavelength, with the same lines as in (a). (c) Spectral density of the spanwise velocity for various wavelengths from $\lambda_z^+ = 2\times10^3$ to $\lambda_z = 10h$, from blue to red, integrated in λ_x over the diagonal band in Fig 6, defined as $\lambda_x \in [2,\ 20]\lambda_z$. The symbols are the perturbation equilibrium profile in Eq. (10), computed from the mean velocity profile in[24]. (d) Friction velocity perturbation intensities obtained from (c). (·····and ▽) Channel[22], $Re_\tau = 550$; the rest are channels[24]: (–·–·– and □) $Re_\tau = 1000$; (– – – and ○) $Re_\tau = 2000$; (——— and △) $Re_\tau = 5200$.

VI. DISCUSSION AND CONCLUSIONS

In summary, we have seen that, as most things in turbulence, the near-wall region is a multi-scale flow involving wide ranges of length and width. In consequence, the near-wall peak of the stream- and spanwise velocity fluctuation intensities cannot be modeled as an elemental object. There is a viscosity-dominated spectral core, centered at $\lambda_x^+ \times \lambda_z^+ \approx 1000\times100$, which embodies the classical turbulence cycle and scales well across Reynolds numbers, and a large-scale component that behaves very differently. The high-Reynolds-number limit of the energy depends on those large scales, which we have explored using spectra. It turns out that they behave near the wall as internal equilibrium boundary layers, driven by the outer large eddies[5,33]. Although this means that they are not essentially different from the mean flow, and share with it the scaled mean profile and physical parameters, they mimic oscillating Stokes layers when they are expressed as fluctuations in a Fourier expansion, and become part of what is known at low Reynolds numbers as the near-wall fluctuation peak.

The intensity of these large-scale fluctuations is predicted to increase logarithmically with Re_τ when expressed in wall units, at least within the Reynolds number range of available experiments, but not to remain concentrated near the wall. At extremely large Reynolds numbers, they should spread to a fraction of the channel thickness, of the order $O(h/5)$. We have shown that their profile can be extracted at laboratory Reynolds numbers from the vertical structure of the spectrum at particular wavelengths. When extrapolated to geophysical Reynolds numbers, they result in a fairly different fluctuation profile, interestingly including a second maximum away from the wall.

In fact, the natural consequence of a model in which most of the near-wall kinetic energy at high Reynolds number is due to interactions with the outer flow is that even this near-wall region, and any part the boundary layer whose distance from the wall is fixed in wall units, should be considered as directly driven by the outer flow. Under those circumstances, and even if the velocity scale for the active turbulence motions responsible for the Reynolds stresses at a given distance from the wall continues to be the friction velocity, a more natural unit for the integrated inactive motions may be some measure of the driving velocity (U_∞, U_{bulk} or some velocity combination such as the mixed scaling in Ref. 6). It is interesting to note that, if we recall from Eq. (1) that $U_\infty \sim \log Re_\tau$, even a logarithmic growth of $u_p'^{2+}$ implies that $u_p'/U_\infty \sim \log^{-1/2} Re_\tau \to 0$ as $Re_\tau \to \infty$. The nature of the singularity is not that u_p' tends to infinity, but that u_τ tends to zero faster than u_p'.

ACKNOWLEDGMENTS

This work was supported by the European Research

Council under the Caust grant ERC-AdG-101018287. I am grateful to R. Deshpande, G. Kunkel, M.K. Lee and I. Marusic for the use of their original data, and to S. Pirozzoli for his thoughtful critique of an early version of this manuscript.

[1]A. N. Kolmogorov, "The local structure of turbulence in incompressible viscous fluid for very large Reynolds numbers," Dokl. Akad. Nauk SSSR **30**, 209–303 (1941).
[2]L. Onsager, "Statistical hydrodynamics," Nuovo Cimento Suppl. **6**, 279–286 (1949).
[3]H. Tennekes and J. L. Lumley, *A first course in turbulence* (MIT Press, 1972).
[4]C. B. Millikan, "A critical discussion of turbulent flows in channels and circular tubes," in *Proc. 5th Intl. Conf. on Applied Mechanics* (Wiley, 1938) pp. 386–392.
[5]J. Jiménez, "Coherent structures in wall-bounded turbulence," J. Fluid Mech. **842**, P1 (2018).
[6]D. B. deGraaff and J. K. Eaton, "Reynolds number scaling of the flat-plate turbulent boundary layer," J. Fluid Mech. **422**, 319–346 (2000).
[7]I. Marusic, W. J. Baars, and N. Hutchins, "Scaling of the streamwise turbulence intensity in the context of inner-outer interactions in wall turbulence," Phys. Rev. Fluids **2**, 100502 (2017).
[8]X. Chen and K. R. Sreenivasan, "Reynolds number scaling of the peak turbulence intensity in wall flows," J. Fluid Mech. **908**, R3 (2021).
[9]P. Monkewitz, "Asymptotics of streamwise Reynolds stress in wall turbulence," J. Fluid Mech. **931**, A18 (2022).
[10]Y. Hwang, "Near-wall streamwise turbulence intensity as $Re_\tau \to \infty$," Phys. Rev. Fluids **9**, 044601 (2024).
[11]M. M. Metzger and J. C. Klewicki, "A comparative study of near-wall turbulence in high and low Reynolds number boundary layers," Phys. Fluids **13**, 692–701 (2001).
[12]M. M. Metzger, J. C. Klewicki, K. L. Bradshaw, and R. Sadr, "Scaling of near-wall axial turbulent stress in the zero pressure gradient boundary layer," Phys. Fluids **13**, 1819–1821 (2001).
[13]A. A. Townsend, "Equilibrium layers and wall turbulence," J. Fluid Mech. **11**, 97–120 (1961).
[14]A. E. Perry and M. S. Chong, "On the mechanism of wall turbulence," J. Fluid Mech. **119**, 173–217 (1982).
[15]A. E. Perry, S. M. Henbest, and M. S. Chong, "A theoretical and experimental study of wall turbulence," J. Fluid Mech. **165**, 163–199 (1986).
[16]A. J. Smits, B. J. McKeon, and I. Marusic, "High-Reynolds number wall turbulence," Ann. Rev. Fluid Mech. **43**, 353–375 (2011).
[17]R. Deshpande, J. P. Monty, and I. Marusic, "Active and inactive components of the streamwise velocity in wall-bounded turbulence," J. Fluid Mech. **914**, A5 (2021).
[18]P. Monkewitz and H. M. Nagib, "Large-Reynolds-number asymptotics of the streamwise normal stress in zero-pressure-gradient turbulent boundary layers," J. Fluid Mech. **783**, 474–503 (2015).
[19]S. Pirozzoli, "On the streamwise velocity variance in the near-wall region of turbulent flows," J. Fluid Mech. **989**, A5 (2024).
[20]J. C. del Álamo, J. Jiménez, P. Zandonade, and R. D. Moser, "Self-similar vortex clusters in the logarithmic region," J. Fluid Mech. **561**, 329–358 (2006).
[21]S. Hoyas and J. Jiménez, "Scaling of the velocity fluctuations in turbulent channels up to $Re_\tau = 2003$," Phys. Fluids **18**, 011702 (2006).
[22]A. Lozano-Durán and J. Jiménez, "Effect of the computational domain on direct simulations of turbulent channels up to $Re_\tau = 4200$," Phys. Fluids **26**, 011702 (2014).
[23]M. Bernardini, S. Pirozzoli, and P. Orlandi, "Velocity statistics in turbulent channel flow up to $Re_\tau = 4000$," J. Fluid Mech. **742**, 171–191 (2014).
[24]M. K. Lee and R. D. Moser, "Direct numerical simulation of turbulent channel flow up to $Re_\tau \approx 5200$," J. Fluid Mech. **774**, 395–415 (2015).
[25]S. Hoyas, M. Oberlack, S. Kraheberger, F. Alcántara-Ávila, and J. Laux, "Wall turbulence at high friction Reynolds numbers," Phys. Rev. Fluids **7**, 014602 (2022).
[26]H. C. H. Ng, J. P. Monty, N. Hutchins, M. S. Chong, and I. Marusic, "Comparison of turbulent channel and pipe flows with varying Reynolds number," Exp. in Fluids **51**, 1261–1281 (2011).
[27]J. Jiménez, S. Hoyas, M. P. Simens, and Y. Mizuno, "Turbulent boundary layers and channels at moderate Reynolds numbers," J. Fluid Mech. **657**, 335–360 (2010).
[28]J. A. Sillero, J. Jiménez, and R. D. Moser, "Two-point statistics for turbulent boundary layers and channels at Reynolds numbers up to $\delta^+ \approx 2000$," Phys. Fluids **26**, 105109 (2014).
[29]J. C. del Álamo and J. Jiménez, "Spectra of very large anisotropic scales in turbulent channels," Phys. Fluids **15**, L41–L44 (2003).
[30]C. E. Willert, J. Soria, M. Stanislas, J. Klinner, O. Amili, M. Elsfelder, C. Cuvier, G. Bellani, T. Fiorini, and A. Talamelli, "Near-wall statistics of a turbulent pipe flow at shear Reynolds numbers up to 40000," J. Fluid Mech. **826**, R5 (2017).
[31]I. Marusic, J. P. Monty, M. Hultmark, and A. J. Smits, "On the logarithmic region in wall turbulence," J. Fluid Mech. **716**, R3 (2013).
[32]J. Jiménez and S. Hoyas, "Turbulent fluctuations above the buffer layer of wall-bounded flows," J. Fluid Mech. **611**, 215–236 (2008).
[33]P. Bradshaw, "Inactive motions and pressure fluctuations in turbulent boundary layers," J. Fluid Mech. **30**, 241–258 (1967).
[34]J. C. del Álamo and J. Jiménez, "Estimation of turbulent convection velocities and corrections to Taylor's approximation," J. Fluid Mech. **640**, 5–26 (2009).
[35]A. Lozano-Durán, O. Flores, and J. Jiménez, "The three-dimensional structure of momentum transfer in turbulent channels," J. Fluid Mech. **694**, 100–130 (2012).
[36]R. J. Adrian, C. D. Meinhart, and C. D. Tomkins, "Vortex organization in the outer region of the turbulent boundary layer," J. Fluid Mech. **422**, 1–54 (2000).
[37]C. D. Tomkins and R. J. Adrian, "Spanwise structure and scale growth in turbulent boundary layers," J. Fluid Mech. **490**, 37–74 (2003).
[38]R. J. Adrian, "Hairpin vortex organization in wall turbulence," Phys. Fluids. **19**, 041301 (2007).
[39]I. Marusic and G. J. Kunkel, "Streamwise turbulence intensity formulation for flat-plate boundary layers," Phys. Fluids **15**, 2461–2464 (2003).
[40]J. Jiménez and P. Moin, "The minimal flow unit in near-wall turbulence," J. Fluid Mech. **225**, 213–240 (1991).
[41]J. M. FmetzHamilton, J. Kim, and F. Waleffe, "Regeneration mechanisms of near-wall turbulence structures," J. Fluid Mech. **287**, 317–348 (1995).
[42]F. Waleffe, "On a self-sustaining process in shear flows," Phys. Fluids **9**, 883–900 (1997).
[43]G. J. Kunkel, *An experimental study of the high Reynolds number boundary layer*, Ph.D. thesis, Aerospace Engng. and Mech., U. Minnesota (2003).
[44]J. R. Garratt, "The internal boundary layer – a review," Bound. Lay. Meteorol. **50**, 171–203 (1990).
[45]E. A. Bou-Zeid, W. Anderson, G. G. Katul, and L. Mahrt, "The persistent challenge of surface heterogeneity in boundary-layer meteorology: a review," Bound. Lay. Meteorol. **177**, 227–245 (2020).
[46]M. Li, C. M. de Silva, D. Chung, D. I. Pullin, I. Marusic, and N. Hutchins, "Modelling the downstream development of a turbulent boundary layer following a step change of roughness," J. Fluid Mech. **949**, A7 (2022).
[47]A. Lozano-Durán and J. Jiménez, "Time-resolved evolution of coherent structures in turbulent channels: characterization of eddies and cascades," J. Fluid Mech. **759**, 432–471 (2014).
[48]I. Marusic, R. Mathis, and N. Hutchins, "Predictive model for wall-bounded turbulent flow," Science **329**, 193–196 (2010).
[49]J. Jiménez, "Cascades in wall-bounded turbulence," Ann. Rev. Fluid Mech. **44**, 27–45 (2012).
[50]P. R. Spalart, "Direct simulation of a turbulent boundary layer

up to $Re_\theta = 1410$," J. Fluid Mech. **187**, 61–98 (1988).
[51] M. M. Metzger, B. J. McKeon, and H. Holmes, "The near-neutral atmospheric surface layer: turbulence and non-stationarity," Phil. Trans. R. Soc. A **365**, 859–876 (2007).
[52] G. K. Batchelor, *The theory of homogeneous turbulence* (Cambridge U. Press, 1953).